Resonant interaction of energetic ions with bulk-ion plasma micro-turbulence

A. Di Siena,[1, a)] T. Görler,[1] E. Poli,[1] R. Bilato,[1] H. Doerk,[1] and A. Zocco[2]

[1)] *Max Planck Institute for Plasma Physics Boltzmannstr 2 85748 Garching Germany*

[2)] *Max Planck Institute for Plasma Physics Wendelsteinstr 1 17491 Greifswald Germany*

(Dated: 9 April 2019)

A significant fast-ion-induced stabilization is observed in linear and nonlinear GENE gyrokinetic simulations which can be attributed to a resonant interaction between energetic particles and the main-ion-temperature-gradient driven plasma turbulence. Elaborating on the findings in [A. Di Siena et al. Nucl. Fusion **58** 054002 (2018)], a detailed study of this mechanism is conducted for realistic JET-like parameters. In view of further exploitation of the beneficial role of energetic ions and corresponding confinement optimization, linear scans over the main fast ion parameters and magnetic plasma geometry are performed. All of these results can be reproduced with a reduced Vlasov-Poisson theoretical model and be explained in terms of modifications on the fast ion energy production/dissipation in the energy balance equation. Finally, despite the essentially linear nature of the resonant interaction, a corresponding nonlinear analysis is also performed and its main dependences captured with a quasi-linear model.

[a)] Electronic mail: alessandro.di.siena@ipp.mpg.de

I. INTRODUCTION

The understanding of the complex turbulent dynamics of magnetically confined plasmas represents one of the most challenging topics in fusion physics. It is particularly relevant to effectively design and optimize future fusion devices, where turbulence will be intrinsically driven by finite density and temperature gradients in conjunction with magnetic-field curvature[1]. In particular, in the typical plasma core conditions the ion-temperature-gradient (ITG) instability[2] is very often identified as the main driver of micro-turbulence. The most detrimental aspect of plasma turbulence for such devices is represented by the associated so-called anomalous particle and heat transport which limits the energy confinement and performance. Therefore, any insight in mechanisms able to systematically suppress them would be highly beneficial. In this context, experimental[3–5] and dedicated numerical studies[6–13] have reported strong fast ions effects on plasma turbulence. Depending on the origin of the energetic tails - e.g. generated through auxiliary heating systems such as neutral beam injection (NBI) or ion cyclotron resonance heating (ICRH) or, in view of ITER, from fusion reactions - these effects are found to possibly provide substantial improvements of the overall confinement. Although several aspects of these findings appear to be intrinsically non-linear[10,14], a major contribution to the ITG mode stabilization could recently be related to a wave-fast-ion resonance which adds to the previously identified (linear) effects[6,7,10,11,15]. In particular, Ref. 13 demonstrated that an effective energy transfer - leading possibly to significant turbulence reduction - occurs if the frequency of the main micro-instability matches the energetic particle magnetic-drift frequency. The analytic predictions of Ref. 13, based on a reduced simplified model, suggested this resonant interaction to be strongly dependent on many energetic ion parameters and plasma geometry. Therefore, to fully explore and more effectively identify the parameter range which could lead to

further turbulence stabilization, a more comprehensive investigation is presented in this work. The corresponding numerical studies are performed with the gyrokinetic code GENE[16] employing realistic plasma parameters inspired by the JET L-mode hybrid discharge of Ref. 10 and 17. All the numerical results are compared with the analytic predictions of a simplified Vlasov model, able to capture the impact of the different parameters on the phase-space position of the resonant interaction. The consequences of such modifications on the energetic particle response are also analyzed in terms of changes in the energy production and/or dissipation in the energy balance equation. The weakening of the thermal ion drive via resonant interaction with energetic particle and the consequent stabilization of the dominant ITG mode is also confirmed in GENE turbulence simulation. Moreover, the nonlinear features of the fast ion heat fluxes are also investigated and reproduced with a quasi-linear model, which extends the simplified theory of Ref. 13. The impact of similar resonance effects in the absence of energetic particles on the thermal ITG micro-instability is discussed in Ref. 18.

In detail, this paper is organized as follows. The plasma scenario and the numerical parameters are described in section II, where first linear scans are shown. The detailed analytic derivation of the reduced simplified model of the energetic particle species is discussed in section III, IV. Hereafter, the impact of the magnetic shear, energetic particle mass and charge is investigated, respectively, in sections V, VI and further extension to turbulent regimes if given in sections VII, VIII.

II. NUMERICAL SIMULATIONS AND PARAMETERS

GENE is a nonlinear Eulerian gyrokinetic code which solves the Vlasov-Maxwell's equations self-consistently on a field-aligned coordinate system $(x, y, z, v_{\shortparallel}, \mu)$. Here, x represents the radial, y the bi-normal and z the magnetic-field-aligned coordinates

in configuration space, while $v_{\shortparallel}$ and μ denote the velocity component parallel to the background magnetic field B_0 and the magnetic moment. Exploiting a δf approach, the fluctuating part of the distribution F_1 is evolved on top of a stationary background F_0 for each plasma species. Although the code has been recently extended to support arbitrary non-Maxwellian distribution functions[19–21], each species background is here approximated as an equivalent Maxwellian for simplicity.

In the following section, linear electrostatic simulations are performed studying the impact of fast particles on the electrostatic ITG micro-instability. The code has been used as an initial value solver, artificially exciting a perturbation at a fixed wave number and studying the linear growth rate of the most unstable solution. The plasma parameters are taken from the JET L-mode hybrid discharge considered in Refs. 10 and 17 and are displayed in Tab. I. Concerning numerical parameters, 32 grid points have been employed in radial direction and 24 along the field line. In velocity space, 32 points and 24 equidistant symmetric grid points have been used for resolving the μ and the $v_{\shortparallel}$ space with a $(\mu, v_{\shortparallel})$ box size of $(9, 3)$ in normalized units. The thermal species are deuterium and electrons while the energetic ions are the ^3He minority species, heated at the fundamental ion-cyclotron (IC) resonance. All the simulations presented in this work are performed retaining shaping effects as provided by the Miller flux-tube magnetic equilibrium[22] with parametrization taken from Ref. 10. The equilibrium is kept fixed for all the numerical analyses performed in this paper. Moreover, collisions are modelled using a linearized Landau-Boltzmann operator[23]. All the simulations presented in this work have been performed with kinetic electrons and realistic deuterium/electron mass ratio. Fig. 1 shows the most unstable linear growth rates as a function of the fast ^{3}He temperature for different values of the wave number $k_y\rho_s$. The growth rates are normalized to c_s/a, with a the minor radius of the device. Here, $c_s = \sqrt{T_e/m_i}$ represents the sound speed, $\rho_s = c_s/\Omega_s$ the thermal gyroradius with $\Omega_s = qB_0/mc$, c is the speed of light, and

TABLE I. Realistic JET L-mode magnetic and plasma parameters. Here, T represents the temperature normalized to the electron one, $R/L_{T,n}$ the normalized logarithmic temperature and density gradients and ν^* the electron-ion collision frequency normalized to the trapped electron bounce frequency.

R	$\hat{s}$	q	T_e/T_i	R/L_{T_i}	R/L_{T_e}
3.1	0.5	1.7	1.0	9.3	6.8
R/L_{n_e}	ν^*	$n_{^3He}$	$R/L_{T_{^3He}}$	$R/L_{n_{^3He}}$	β_e
1.3	0.038	0.07	23.1	1.6	0

m and q (not to be confused with the safety factor in Tab. I) are the ion mass and charge, respectively. In contrast with the standard dilution theory, which predicts a dependence only on the fast particle charge concentration, the linear ITG growth rates are found to be strongly affected by the different fast particle temperatures (T_f). In particular, Fig. 1 reveals a pronounced temperature dependence of the ITG linear growth rates with a maximum relative reduction of ca. 50% compared with the case of thermal helium. Moreover, the temperature of the energetic particles corresponding to the highest stabilization varies significantly with the bi-normal wave vector ($k_y\rho_s$). This observation is particularly relevant in view of turbulence simulations, where different modes are coupled through a cross-scale nonlinear operator. Hence, at a fixed temperature, each scale undergoes a different resonant stabilization. Furthermore, a common feature observed in Fig. 1 is that dilution (identified by the black line in each figure) is always recovered at very large temperatures. These results suggest a dynamic fast ion effect on the linear ITG modes that, above a certain threshold, weakens with the energetic particle temperature. Regarding the mode frequencies, smaller changes are observed, with a relative variation of $\sim 25\%$ compared with the thermal helium case. It should be remarked that at the nominal

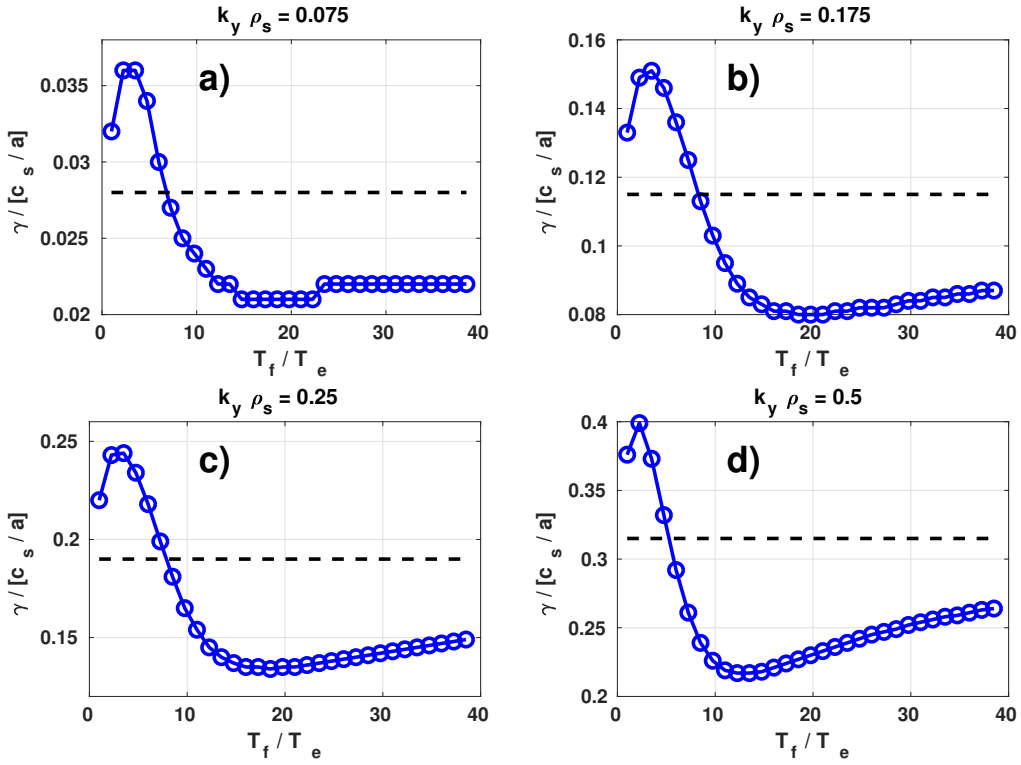

FIG. 1. Growth rates as a function of the fast particle temperature T_f/T_e for a) $k_y\rho_s = 0.075$, b) $k_y\rho_s = 0.175$, c) $k_y\rho_s = 0.25$ and d) $k_y\rho_s = 0.5$. The dashed black line represents the pure dilution growth rate, obtained by retaining the energetic particles only in the zero order quasi-neutrality equation.

fast-ion to electron temperature ratio ($T_f/T_e \simeq 6.9$ for the reference plasmas we are considering), the fast-ion effect described in this paper is rather weak, which may explain why it had not been noted before the analysis presented in Ref. 13.

These results are further corroborated by the study of the phase angle (α) between the electrostatic potential ϕ_1 and main ion density perturbation. Fig. 2 shows α for different fast ion temperatures at the specific choice of $k_y\rho_s = 0.5$. In case

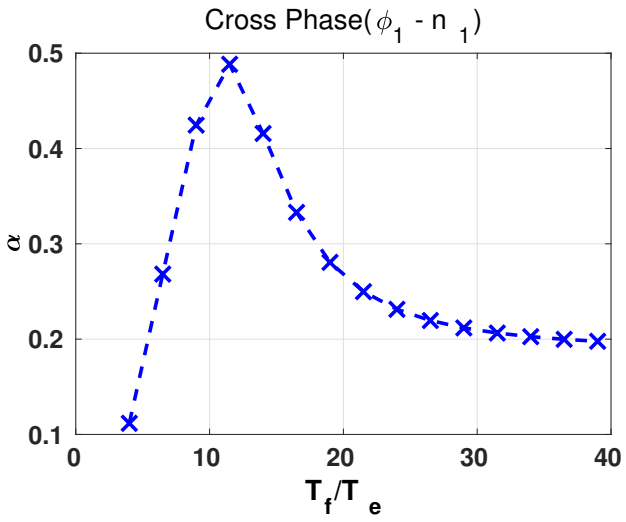

FIG. 2. Cross phases (in rad) between the perturbed electrostatic potential and the main ion density perturbation at $k_y\rho_s = 0.5$ as function of the fast particle temperature.

of no active interaction between the fast particles and the main drive of the ITG instability (e.g. only dilution), a constant cross phase would be expected for different fast particle temperatures. However, a varying behaviour is observed in Fig. 2, where fast particles significantly modify the electrostatic field ϕ_1. The maximum of this interaction is always observed in correspondence with the maximum growth rate stabilization, which for $k_y\rho_s = 0.5$ is at $T_f = 12T_e$. For this temperature, the fast helium strongly affects the main instability and impacts the electrostatic field both in terms of magnitude and phase. In simulations without energetic particles a zero cross phase angle α is obtained.

III. REDUCED ENERGETIC ION VLASOV EQUATION

The linear, electrostatic numerical setup employed in the previous section allows us to further investigate the energetic particle effects on plasma micro-turbulence with a simplified analytic model. In the gyrokinetic code GENE, the most unstable linear growth rates are computed by consistently solving the Vlasov equation for each plasma species and the electrostatic field component ϕ_1. Fast ion effects on the most unstable linear mode are hence represented by modifications of the thermal species response to any external perturbation in the normalized Poisson field equation

$$\phi_1(\mathbf{x}) = \frac{\sum_s q_s \pi n_{0,s} B_0 \int J_0(\lambda_s) F_{1,s}(\mathbf{x}) \, dv_{\shortparallel} d\mu}{\left[k_\perp^2 \lambda_{De}^2 - \sum_s \frac{\pi q_s^2 n_{0,s}}{T_{0,s}} \int (1 - J_0^2(\lambda_s)) \frac{\partial F_{0,s}}{\partial \mu} dv_{\shortparallel} d\mu\right]}, \tag{1}$$

with $k_\perp$ the wave vector component perpendicular to the background magnetic field, $\lambda_{De} = \sqrt{T_e/(4\pi\rho_s^2 n_e e^2)}$ the normalized Debye length, J_0 the zero-order Bessel function, $\lambda_s = (k_\perp/q_s)\sqrt{2m_s\mu/B_0}$, s the plasma species index and F_0 the generic energetic particle background distribution function. Furthermore, the reference values used to normalize Eq. (1) are the elementary electron charge e, the main ion mass m_i, the electron temperature T_e, the on-axis magnetic field B_0 and the minor radius. A detailed derivation of Eq. (1) can be found in Ref. 23. The energetic particle contribution in Eq. (1) is determined by the zero-order moment of their perturbed distribution function $F_{1,f}$. It evolves in time accordingly to the Vlasov equation, which in the GENE field aligned coordinate system (x, y, z) reads

$$\begin{aligned}\frac{\partial F_{1,f}}{\partial t} = &-\frac{C}{JB_0} v_{th,f} v_{\shortparallel} \left[\partial_z F_{1,f} - \frac{q_f}{2T_f v_{\shortparallel}} \partial_z \bar{\phi}_1 \frac{\partial F_0}{\partial v_{\shortparallel}}\right] + \frac{C}{JB_0} v_{th,f} \frac{\mu}{2} \partial_z B_0 \frac{\partial F_{1,f}}{\partial v_{\shortparallel}} \\ &- \frac{T_f}{q_f}\left(\frac{\mu B_0 + 2v_{\shortparallel}^2}{B_0}\right) \mathcal{K}_x \left[\partial_x F_{1,f} - \frac{q_f}{2T_f v_{\shortparallel}} \frac{\partial F_0}{\partial v_{\shortparallel}} \partial_x \bar{\phi}_1\right] \\ &- \frac{T_f}{q_f}\left(\frac{\mu B_0 + 2v_{\shortparallel}^2}{B_0}\right) \mathcal{K}_y \left[\partial_y F_{1,f} - \frac{q_f}{2T_f v_{\shortparallel}} \frac{\partial F_0}{\partial v_{\shortparallel}} \partial_y \bar{\phi}_1\right] - \frac{1}{C} \hat{\partial}_x F_0 \partial_y \bar{\phi}_1.\end{aligned} \tag{2}$$

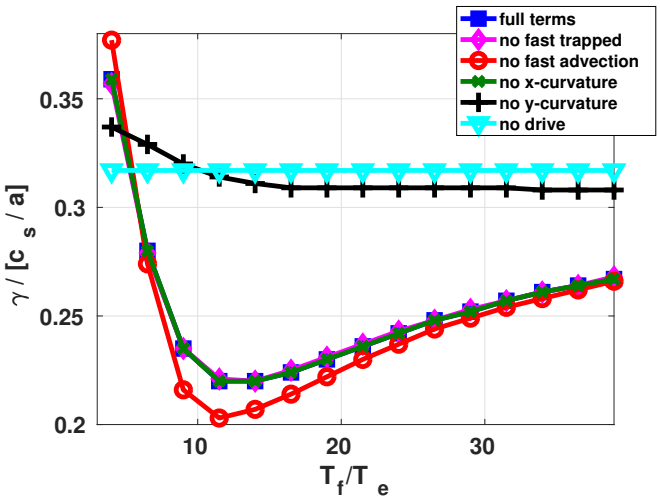

FIG. 3. Growth rates obtained by artificially suppressing different terms in the fast particle Vlasov equation at $k_y\rho_s = 0.5$.

Here, $\mathcal{K}_x = -((\mathbf{B}_0 \times \nabla B_0) \cdot \hat{x})/B_0^2$, $\mathcal{K}_y = -((\mathbf{B}_0 \times \nabla B_0) \cdot \hat{y})/B_0^2$, $\mathcal{C}^2 = \mathbf{B}_0 \cdot \mathbf{B}_0$ and $\mathcal{J}^{-1} = \mathbf{B}_0 \cdot \nabla z/\mathcal{C}$. Furthermore, $\bar{\phi}_1 = J_0(\lambda)\phi_1$ denotes the gyroaveraged potential. The neoclassical terms have been neglected, since they are not expected to affect the time evolution of $F_{1,f}$ and furthermore evolve entirely independently in the flux-tube limit. The individual right hand side terms of Eq. (2) are hence the parallel advection, the trapped particle, the radial (x) and bi-normal (y) curvature and the background drive. The contribution of each of these terms to the overall fast-ion effect observed in Fig. 1- 2 can be investigated by artificially suppressing them in GENE. Fig. 3 demonstrates that the trapped fast-particle, the parallel dynamic and the radial curvature terms play only a minor role in the linear ITG growth rate stabilization for the ^{3}He setup. Similar results are also observed in different plasma regimes and numerical setups[24,25].

A reduced simplified expression for the energetic ion Vlasov equation able to

qualitatively capture the temperature dependences shown in Fig. 3 can hence be derived by removing all the negligible terms from Eq. (2),

$$\frac{\partial F_{1,f}}{\partial t} = -\frac{T_0}{q}\left(\frac{\mu B_0 + 2v_{\shortparallel}^2}{B_0}\right)\mathcal{K}_y \partial_y F_{1,f} + \left[\frac{1}{2v_{\shortparallel}}\frac{\partial F_0}{\partial v_{\shortparallel}}\left(\frac{\mu B_0 + 2v_{\shortparallel}^2}{B_0}\right)\mathcal{K}_y - \frac{1}{C}\hat{\partial}_x F_0\right]\partial_y \bar{\phi}_1. \tag{3}$$

Eq. (3) is the gyrokinetic solution used to investigate the resonant effect of magnetic curvature in setting the linear threshold of ITG, in general toroidal geometry[18]. Employing a plane wave ansatz for the perturbed quantities, i.e. the electrostatic potential ϕ_1 and the perturbed distribution function F_1,

$$\phi_1(x, y, z) = \sum_{k_x, k_y} \phi_1(k_x, k_y, z) e^{-i\omega t + i(k_x x + k_y y)}, \tag{4}$$

the following simplified Vlasov equation for each wave vector $\mathbf{k}$ and frequency $\omega = -\omega_r + i\gamma_\nu$ can be derived

$$F_{1,f} = \frac{k_y \bar{\phi}_1 \left[\frac{1}{2v_{\shortparallel}}\frac{\partial F_0}{\partial v_{\shortparallel}}\left(\frac{\mu B_0 + 2v_{\shortparallel}^2}{B_0}\right)\mathcal{K}_y - \frac{1}{C}\hat{\partial}_x F_0\right]}{\omega_r - i\gamma_\nu + \frac{T_f}{q}\left(\frac{\mu B_0 + 2v_{\shortparallel}^2}{B_0}\right)k_y \mathcal{K}_y}. \tag{5}$$

The real frequency ω_r is defined with a minus sign to account for the default sign convention in GENE where positive values indicate modes propagating in the ion diamagnetic-drift direction. Furthermore, for all the simulations performed in this work, the term $\partial F_0/\partial v_{\shortparallel}\mathcal{K}_y\left(\mu B_0 + 2v_{\shortparallel}^2\right)/(2v_{\shortparallel}B_0)$ is found to be negligible if compared to $\left(\hat{\partial}_x F_0\right)/C$ and is erased for the rest of the theoretical analysis. Although a simplified isotropic Maxwellian distribution function is employed throughout this paper to model the energetic particle population, Eq. (5) is written for a general background distribution function F_0. For the specific choice of an equivalent Maxwellian distribution, the x- and $v_{\shortparallel}-$derivative terms evaluate to

$$\hat{\partial}_x F_M = \left[\frac{R}{L_n} + \frac{R}{L_T}\left(v_{\shortparallel}^2 + \mu B_0 - \frac{3}{2}\right)\right]F_M, \tag{6}$$

and

$$\frac{1}{2v_{\shortparallel}}\frac{\partial F_M}{\partial v_{\shortparallel}} = -F_M \tag{7}$$

in normalized units. Eq. (5) reveals that the perturbed part of the energetic ion distribution function depends mainly on the background drive, i.e. density and temperature gradients, and on the bi-normal curvature terms. In particular, as explained in detail in Ref. 13, a resonance occurs if the real frequency of the main micro-instability, ω_r, matches the magnetic-drift frequency of the energetic particle species $\omega_{d,f}$, defined by the right-hand side of

$$\omega_r = \frac{T_f}{q}\left(\frac{\mu B_0 + 2v_{\shortparallel}^2}{B_0}\right) k_y \mathcal{K}_y. \tag{8}$$

If this condition is fulfilled, energy can be effectively exchanged between the energetic particles and the bulk-ion micro-instability. It is worth specifying that $\omega_{d,f}$ depends on the fast ion temperature and charge, and has a complex 3D structure in $(z, v_{\shortparallel}, \mu)$. Eq. (8) reveals that the y-curvature term $\mathcal{K}_y$ must be negative to match the resonance condition. A constraint over the field-aligned angle is then identified by studying the structure of $\mathcal{K}_y$, see Sec. V. These analytic predictions are confirmed by GENE numerical results[13].

IV. FAST PARTICLE GROWTH RATE CONTRIBUTION

According to the reduced Vlasov model developed in the previous section, a resonance between energetic particles and micro-turbulence is expected if the linear frequency of the bulk-ion mode approaches the fast ion magnetic-drift frequency. Correspondingly, a net energy transfer between wave and particles occurs. Both the direction and magnitude of the energy exchange can be investigated for each values of the fast particle temperature through the time evolution of the system free energy

E_{fe}. The latter is defined – similarly to the standard fluid theory – as the sum of the kinetic E_k and field E_w contributions[26,27],

$$E_k = \sum_s \Re \left\{ \int dz d\mu dv_{\shortparallel} \frac{\pi B_0 n_{0,s} T_{0,s}}{2F_{0,s}} |F_{1,s}^k|^2 \right\}, \tag{9}$$

$$E_w = \sum_s \Re \left\{ \int dz d\mu dv_{\shortparallel} \frac{\pi B_0 q_s n_{0,s}}{2} \bar{\phi}_1^{k,*} F_{1,s}^k \right\}. \tag{10}$$

The time derivative of Eqs. 9-10 represents the free energy balance equation, which determines the energy flow in the whole simulation time domain. In steady-state, the overall free energy is conserved, i.e. $\partial E_{fe}/\partial t = 0$. This implies that the time variation of the energy transferred from the wave to the particles ($\partial E_k/\partial t$) and the energy transferred back in the inverse process ($\partial E_w/\partial t$) reaches an equilibrium. As shown in detail in Refs. 27 and 28, the potential and kinetic parts of the overall energy balance can be written as

$$\frac{\partial E_k}{\partial t} = \sum_s \Re \left\{ \int dz d\mu dv_{\shortparallel} \frac{\pi B_0 n_{0,s} T_{0,s}}{F_{0,s}} F_{1,s}^{k,*} \frac{\partial F_{1,s}^k}{\partial t} \right\}, \tag{11}$$

$$\frac{\partial E_w}{\partial t} = \sum_s \Re \left\{ \int dz d\mu dv_{\shortparallel} \pi B_0 q_s n_{0,s} \bar{\phi}_1^{k,*} \frac{\partial F_{1,s}^k}{\partial t} \right\}. \tag{12}$$

An effective linear growth rate[29], related to the exponential growth of the main plasma micro-instability, can be defined starting from Eq. (11), (12),

$$\gamma = \sum_s \gamma_s = \frac{1}{E_w} \sum_s \frac{\partial E_{w,s}}{\partial t}. \tag{13}$$

This definition allows to separate the contribution of each species (s) to the overall linear growth rate and to identify resonance effects in phase space by studying the velocity $\gamma(v_{\shortparallel}, \mu)$-kernel. Here, positive (negative) values of γ_s indicate that the plasma

species considered is giving (taking) energy to (from) the electrostatic field component with a consequent growth (damping) of the mode. A reduced expression for the energetic particle γ_f can be derived by employing the plane wave ansatz defined in the previous section and the simplified fast ion perturbed distribution function $F_{1,f}$ of Eq. (5), namely

$$\gamma_f = -\frac{1}{E_{pot}} \Bigg\{ \int dz dv_{\shortparallel} d\mu \pi n_f J_0^2 |\phi_1^k|^2 T_f \left(v_{\shortparallel}^2 + \mu B_0\right) k_y^2 \mathcal{K}_y \frac{\gamma_\nu}{\mathcal{C}} \frac{\left[\frac{R}{L_{n,f}} + \frac{R}{L_{T,f}} \left(v_{\shortparallel}^2 + \mu B_0 - \frac{3}{2}\right)\right] F_M}{\left(\omega_r + \frac{T_f}{q_f} \left(\frac{\mu B_0 + 2v_{\shortparallel}^2}{B_0}\right) k_y \mathcal{K}_y\right)^2 + \gamma_\nu^2} \Bigg\}. \tag{14}$$

The resulting expression reveals that the energetic ion contribution to the overall energy production or dissipation is maximized in correspondence to the minimum of the denominator of Eq. (5), therefore leading - potentially - to substantial modifications of the bulk instability. As explained in the previous section, the bi-normal curvature term $\mathcal{K}_y$ must be negative in order to fulfill the resonance condition of Eq. (8) in ITG-dominated scenarios. A first direct consequence of this observation is that the sign of γ_f is entirely determined by the radial derivative of the energetic particle background distribution function. Therefore, beneficial (negative) or detrimental (positive) contributions to the overall γ depend on the location in phase space of the resonance and on the corresponding sign of the energetic ion drive. The first term (denominator of Eq. (14), i.e. resonance) amplifies the magnitude of the fast ion contribution to the total growth/damping rate while the second one (numerator of Eq. (14), i.e. drive) determines the direction of the energy exchanged between particles and wave.

These analytic predictions, based on the reduced model of Eq. (14), are confirmed by GENE linear simulations. Fig. 4 shows the ITG growth rate temperature dependences for $k_y \rho_s = 0.1$ and $k_y \rho_s = 0.5$ for positive and negative temperature gradients.

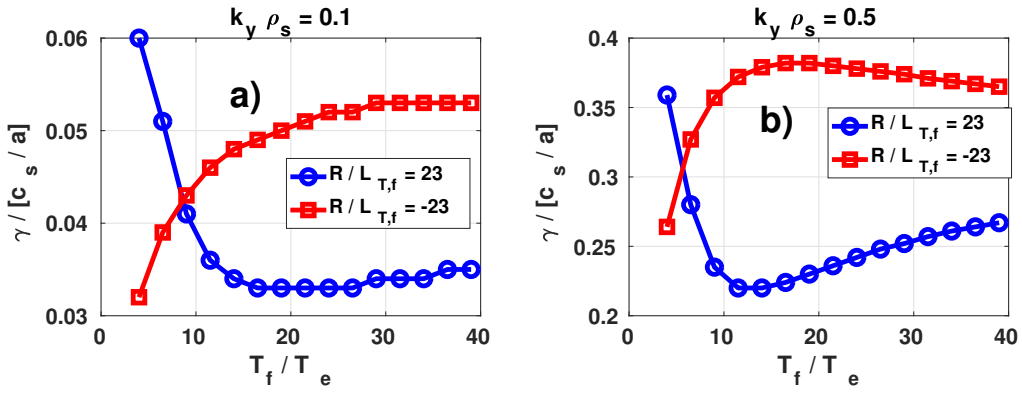

FIG. 4. Growth rates obtained for positive ($R/L_{T,f} = 23$) and negative ($R/L_{T,f} = -23$) values of the fast ion temperature gradients at a) $k_y\rho_s = 0.1$ and b) $k_y\rho_s = 0.5$.

For both values of the bi-normal mode numbers, the fast particle effect on the linear micro-instability goes from stabilizing to destabilizing and vice-versa as the sign of the logarithmic temperature gradient is changed. These results are consistent with the modifications in the direction of the net energy transfer between particles and wave that is predicted with the reduced analytic model of Eq. (14). This can be observed in Fig. 5 where the drive term is shown as a function of $v/v_{th,f}$ for the positive and negative values of the fast particle temperature gradients. Moreover, the change in the sign in $R/L_{T,f}$ does not affect the energetic particle magnetic-drift drift frequency (as shown in Fig. 5). Thus, the resonance position with the bulk-ion micro-instability undergoes only minor modifications due to changes in the real frequency ω_r. The most relevant fast particle contribution to the linear ITG growth rates is observed in correspondence of $T_f \sim 25T_e$ and $T_f \sim 12T_e$, respectively for $k_y\rho_s = 0.1$ and $k_y\rho_s = 0.5$ regardless of the sign of $R/L_{T,f}$. These results are further corroborated by the study of the phase-space structure of the γ_f functions obtained from GENE simulations in Fig. 6 for the case $k_y\rho_s = 0.5$ and $T_f = 12T_e$. This

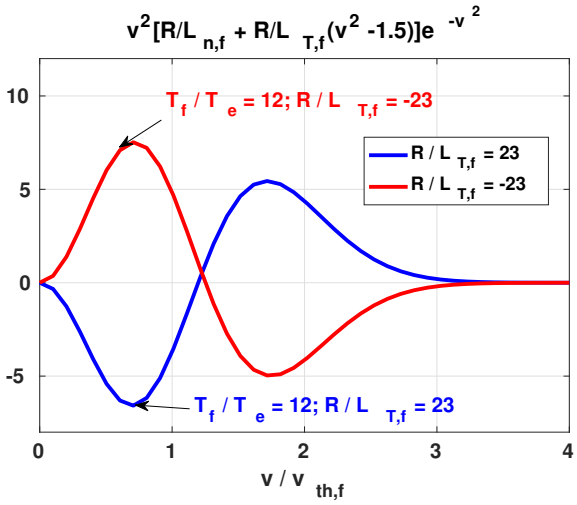

FIG. 5. Cartoon of the drive term contribution in Eq. (14) connected with the wave-fast particle resonance for the positive and negative values of the fast particle temperature gradients. The resonance positions are indicated by the black arrows.

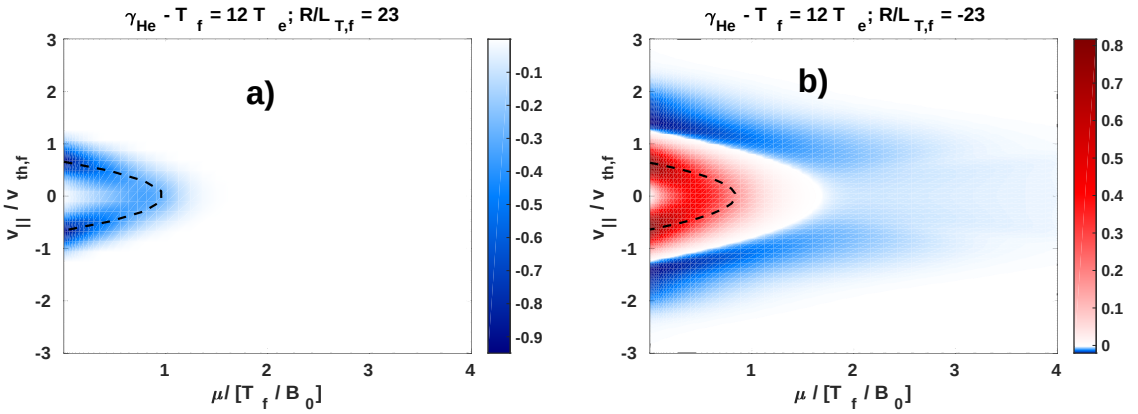

FIG. 6. Converged fast particle γ_f velocity space structure obtained from GENE at $z = 0$, $k_y\rho_s = 0.5$ and $T_f = 12T_e$ for (a) $R/L_{L_{T,f}} = 23$, (b) $R/L_{L_{T,f}} = -23$. The black contour lines indicate the resonance positions according to the reduced Vlasov model.

analysis might be particularly relevant optimizing plasma scenarios where different ICRH schemes can be employed, e.g. on-axis/off-axis. Typically, for off-axis heating, most of the radio-frequency (RF) power is absorbed far from the magnetic axis and the fast-ion temperature gradient is positive on the inner side of the profile, i.e. the corresponding R/L_{Tf} is negative. According to the linear analysis discussed above, the positive and negative parts of the fast-ion drive, see numerator in Eq. (14), are swapped if R/L_{Tf} becomes negative, i.e. a stabilizing contribution is expected at lower temperatures, which turns to destabilizing at higher temperatures. It should be remarked that, for off-axis heating, the power absorbed per particle decreases due to the larger deposition volume and a lower fast-ion temperature can be expected. However, further analyses are required to validate this point. They are planned for the near future.

V. IMPACT OF MAGNETIC SHEAR

The wave-fast ion resonance mechanism described in the previous sections depends strongly on the binormal y-curvature term $\mathcal{K}_y$. It affects the resonance position in phase space and imposes a threshold condition for the particle to interact with the bulk ITG mode. In this section, the role of $\mathcal{K}_y$ will be further analyzed by changing the value of the magnetic shear $\hat{s} = \frac{\rho}{q}\frac{dq}{d\rho}$ on the flux surface labeled by the radial coordinate $\rho = a\sqrt{\Psi_t/\Psi_{t,edge}}$ with the toroidal flux Ψ_t. An analytic first order approximation for $\mathcal{K}_y$ is given in the limit of a simple s-α geometry and reads $\mathcal{K}_y \sim -\cos(z) - \hat{s}z\sin(z)$[24]. It reveals that the main geometrical parameter which determines the shape of the y-curvature term $\mathcal{K}_y$ is the magnetic shear and it does not affect the amplitude of $\mathcal{K}_y$ at $z = 0$. Nevertheless, it strongly impacts the position of its zeroes, as confirmed in Fig. 7 by the realistic geometrical coefficients obtained for the cases $\hat{s} = 0.7$ and $\hat{s} = -0.4$. To analyze the role of the magnetic shear on the

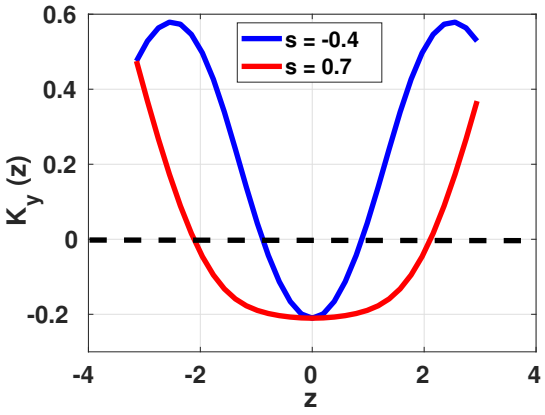

FIG. 7. Geometrical coefficients $\mathcal{K}_y$ extracted from GENE for $\hat{s} = -0.4$ and $\hat{s} = 0.7$. The black line corresponds to $\mathcal{K}_y = 0$.

ITG/energetic particle resonant microturbulence suppression, linear simulations have been performed for $\hat{s} = 0.7$ and $\hat{s} = -0.4$ at different fast ion temperatures. In order to remove any effect of the magnetic shear on the thermal ITG drive and account only for the changes on the resonant fast ion stabilization, the linear growth rates displayed in Fig. 8 are normalized to the ones obtained without energetic particles. The strongest relative fast-ion stabilization is observed for $\hat{s} = -0.4$ (ca. 40%), which exceeds by ca. 10% the one observed at $\hat{s} = 0.7$. Moreover, only mild linear ITG real frequency changes are observed. It is worth mentioning here that as the ITG micro-instability drive reduces with the magnetic shear, the stabilizing effect of energetic particles becomes more relevant. In particular, the fast ion contribution to the linear growth rate normalized to the thermal drive (γ_f/γ_{nf}) increases. These results are consistent with the predictions of the reduced theoretical model introduced before. A decrease in the magnetic shear leads to a further localization of the wave-particle resonance in the bad curvature region (Fig. 7), strengthening the fast ion contribution to the linear growth rates. The thermal ITG is indeed maximum at $z = 0$. To

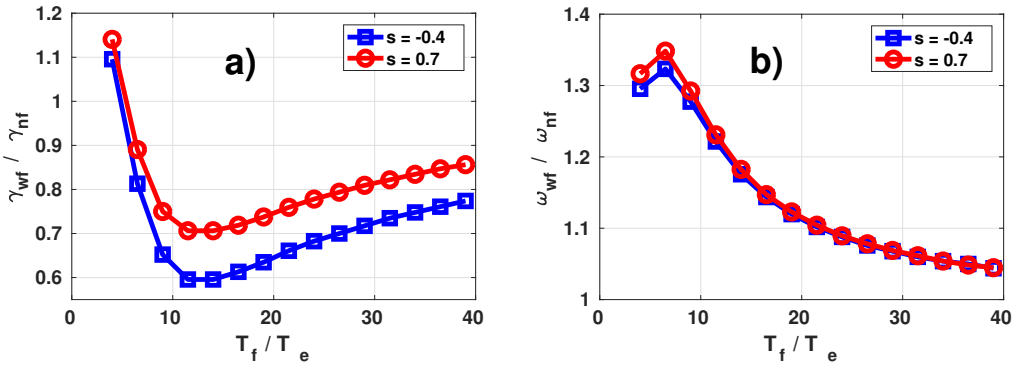

FIG. 8. Ratio between the linear growth rates (a) and real frequencies (b) obtained with and without energetic particles for $\hat{s} = -0.4$ and $\hat{s} = 0.7$ at $k_y\rho_s = 0.5$. The nominal ITG growth rates and frequencies in the absence of fast ions are $\gamma_{nf} = 0.243c_s/a$, $\omega_{nf} = 0.531c_s$ and $\gamma_{nf} = 0.387c_s/a$, $\omega_{nf} = 0.544c_s$, respectively for $\hat{s} = -0.4$ and $\hat{s} = 0.7$.

further corroborate these numerical results, the $z - v_{\shortparallel}$ phase-space structures of the energetic particle curvature contribution to the linear growth rate normalized to the thermal drive in the absence of fast ions (γ_f/γ_{nf}) are shown in Fig. 9 for $s = 0.7$ and $s = -0.4$. The magnetic moment is fixed to $\mu = 0$, which corresponds to the most relevant contribution to the overall γ_f. Consistently with the change in the shape of $\mathcal{K}_y$, Fig. 9 confirms the progressive localization of the resonance position at smaller values of z as the magnetic shear is reduced. The beneficial (negative) region of the energetic particle contribution to the linear growth rate is always delimited by the black dotted line, which represents the resonance position as determined with the reduced model of Eq. (8) (dominated by $\mathcal{K}_y$). This result demonstrates that no resonant interaction is allowed in $z - v_{\shortparallel}$ regions where the y-curvature term assumes positive values. Moreover, the strongest stabilization is observed in regions where the predicted resonance position overlaps the negative fast

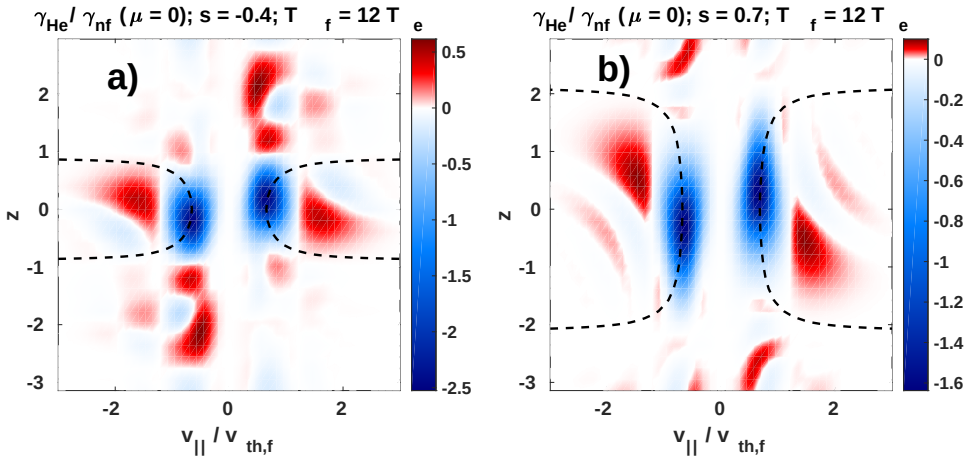

FIG. 9. Converged fast particle contribution to the linear growth rate normalized to the thermal drive γ_f/γ_{nf} obtained from GENE at $\mu = 0$, $k_y\rho_s = 0.5$ and $T_f = 12T_e$ for (a) $\hat{s} = -0.4$, (b) $\hat{s} = 0.7$. The black contour lines indicate the resonance positions according to the reduced Vlasov model. To remove any effect of the magnetic shear on the thermal ITG drive and account only for the changes on the resonant fast ion stabilization, the fast ion contributions to the linear growth rates are normalized to the overall value obtained without energetic particles.

particle drive term. Triangularity, safety factor and other geometrical coefficients are not expected to significantly affect $\mathcal{K}_y$ and hence the energetic particle magnetic-drift frequency. They may, however, influence the bulk ion and electron response and, only afterward, the ITG-energetic particle resonant effects via modifications on the real ITG mode frequencies.

VI. INFLUENCE OF ENERGETIC ION PROPERTIES

In sections II and III, the resonance mechanism presented in this paper has been described with a reduced model able to capture the main dependences observed in the GENE linear simulations. According to this model, the wave-fast ion stabilization is the result of a wave-fast-ion resonance term, which maximizes the otherwise negligible energetic particle contribution in the Poisson equation. Eq. (8) shows that the phase space position of the resonance strongly depends on the charge and mass of the energetic particle species. Aiming for further exploitation of the stabilizing effect, it is hence obvious to explore the impact of the various fast ion properties. Therefore, numerical scans over the fast particles charge (in electron-charge units) and mass (in deuterium-mass units) are performed in the present section, comparing to reference parameters given in Tab. I. Moreover, the analytic predictions of the reduced model, derived in the previous sections, will be further validated.

A. Fast ion charge dependence

The first parameter analyzed here is the fast particle charge. It directly affects the magnetic-drift frequency and thus the phase-space position of the wave-fast particle resonance. Moreover, it enters in the field equation as a weight to the energetic particle density perturbation and modifies the fast particle Larmor radius corrections. The dependence of the fast particle resonant stabilization on the energetic ion charge is investigated in this section with linear electrostatic simulations. The reference physical parameters are the same as in Tab. I for each value of the fast particle charge employed throughout this section, which is the only parameter changed. Moreover, the charge concentration is always kept fixed to the value $q_f n_f = 0.14 n_e$. The choice of keeping a constant charge concentration is particularly convenient to

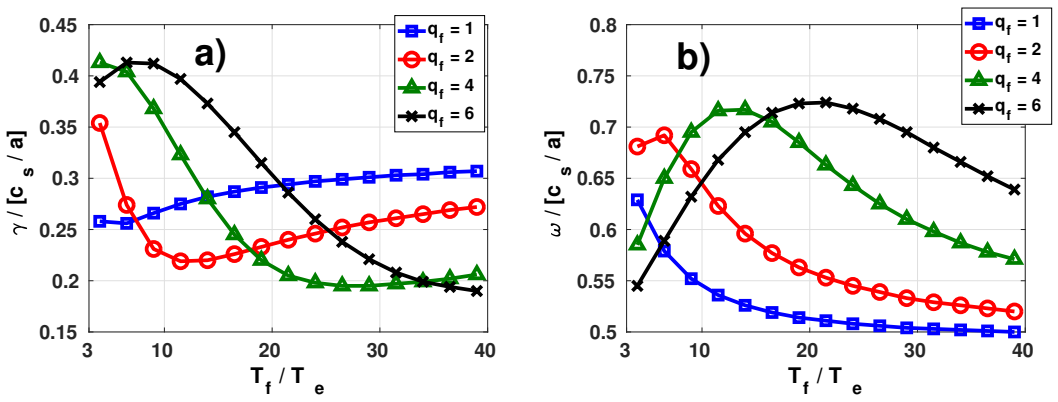

FIG. 10. a) Growth rates and b) frequencies as a function of the fast particle temperature T_f/T_e and charge q_f at $k_y\rho_s = 0.5$. The fast particle charge concentration is fixed to $q_f n_f = 0.14 n_e$.

isolate the charge dependence of the resonance mechanism from other electrostatic physical effects, i.e. mainly dilution. Fig. 10 shows the temperature behaviour of the linear ITG growth rates and frequencies for different values of q_f. It reveals that the charge of fast particles can significantly affect the growth rate, with relative changes up to 50%. The real frequency, on the other hand, experiences weaker modifications of about 20%. In particular, the strongest linear growth rate reduction is observed for the largest energetic particle charge, which is consistent with the reduction of the argument of the zero order Bessel functions. For the same charge concentration, an increase in the fast ion charge is hence reflected in a corresponding increment in the energetic particle contribution in the Poisson field equation and thus to an increase of its beneficial effect. However, arbitrarily high charge would be unrealistic in experimental conditions and a corresponding optimization would need to consider further limitations. Another interesting observation is that the energetic particle temperature corresponding to the minimum of the linear growth rates moves towards higher

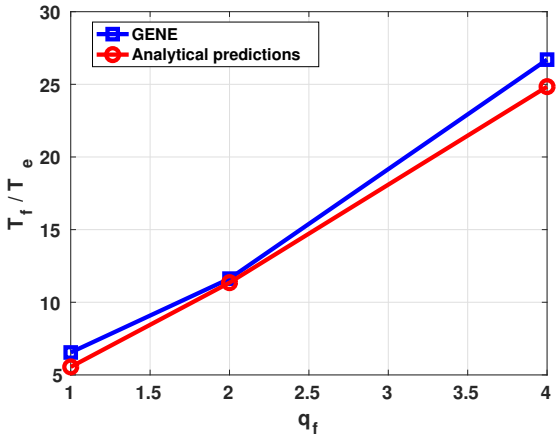

FIG. 11. Comparison of the numerical (GENE - blue line) and analytic predictions (red line) of the fast ion temperature corresponding to the most stable linear growth rate for different fast particle charge. The fast particle charge concentration is fixed to $q_f n_f = 0.14 n_e$.

values as the fast ion charge increases. This result is in agreement with the theoretical predictions of the reduced model of Eq. (5), (8). In the limit for which the mode frequency is only slightly affected by the change in the fast particle charge, Eq. (8) imposes a constraint over the fast ion temperature required to fulfill the resonance interaction, i.e. the ratio T_f/q_f must be kept constant. Fig. 11 shows a particular good agreement between the numerical GENE results and the analytic prediction of the optimal fast ion temperature which maximizes the ITG linear suppression. The frequencies used in the analytic model are taken from the GENE simulations.

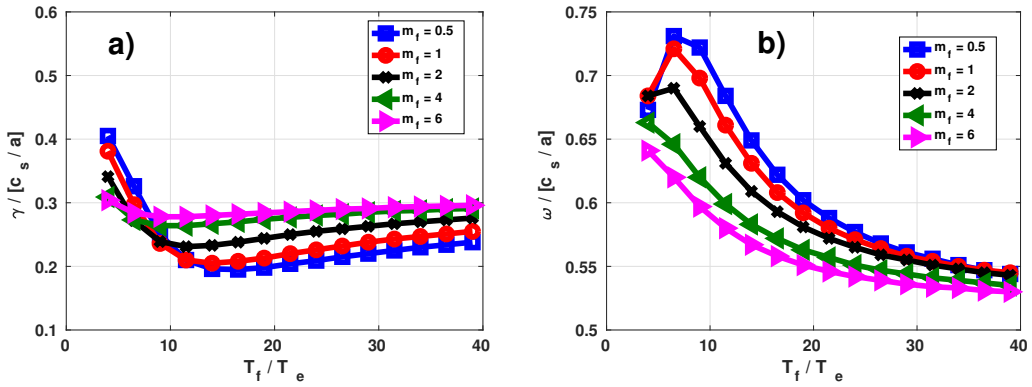

FIG. 12. a) Growth rates and b) frequencies as a function of the fast particle temperature T_f/T_e and mass m_f at $k_y\rho_s = 0.5$. The fast particle charge concentration is fixed to $q_f n_f = 0.14 n_e$.

B. Fast ion mass dependence

A second parameter which characterizes different fast ion species is their mass (m_f), which is not expected to significantly affect the resonance position according to the reduced theoretical model presented previously. Nevertheless, it enters in the argument of the Bessel functions. In particular, an increase in m_f leads to larger finite Larmor radius effects and thus to smaller energetic particle contributions to the overall electrostatic field. The impact of the mass on the linear growth rates and frequencies is shown in Fig. 12. The physical parameters are the same of Tab. I and the charge concentration is kept to $q_f n_f = 0.14$. As predicted, the magnitude of the linear ITG growth rate reduction decreases by increasing the fast particle mass and almost disappears for the value of $m_f = 6$. This results align well with the experimental need to use light energetic ions. Moreover, Fig. 12 shows only minor modifications on the fast ion temperature related to the more effective ITG

stabilization. These results are in agreement with the theoretical predictions, where only minor modifications are expected due to changes in the real frequency ω_r of the more unstable mode.

C. Combined effect of fast ion charge and mass

The identification of the fast particle species which maximizes the ITG/fast-ion beneficial interaction is addressed in this section. The balance of the complex effects of mass - that increases the argument of the Bessel function as $\sqrt{m_f}$ - and charge - which impacts on the position of the resonance and reduces the argument of the Bessel function- is investigated. Fig. 13 shows the linear temperature dependences of growth rates in a three species setup with deuterium, electron and different fast ion species, considered as ^{2}D, ^{3}He, ^{7}Li and ^{9}Be. Here, the fast particle charge concentration is fixed at $q_f n_f = 0.14$. The parameters are the same as in Tab. I and the bi-normal wave number is chosen at the maximum ITG growth rate, namely $k_y\rho = 0.5$. Fig. 13 reveals that the most stable growth rates change significantly with the fast particle species. In particular, at $T_f < 9T_e$, the minimum ITG linear growth rate is observed for the fast deuterium. In the range between $9 < T_f/T_e < 20$ helium shows the highest stabilization while lower growth rates are observed for beryllium at higher temperature. In Fig. 13 the black cross on each line corresponds to maximum fast ion stabilization predicted with Eq. (8). The predicted fast ion temperature related to the maximum stabilization and the numerical GENE results are in perfect agreement. Only minor modifications on the ITG mode frequencies are instead observed. As already mentioned before, these results depend significantly on the fast particles temperature, density gradients and on the magnetic geometry. The numerical analysis presented in this section relies on the assumption that the different energetic particle species have the same gradients and have the same impact

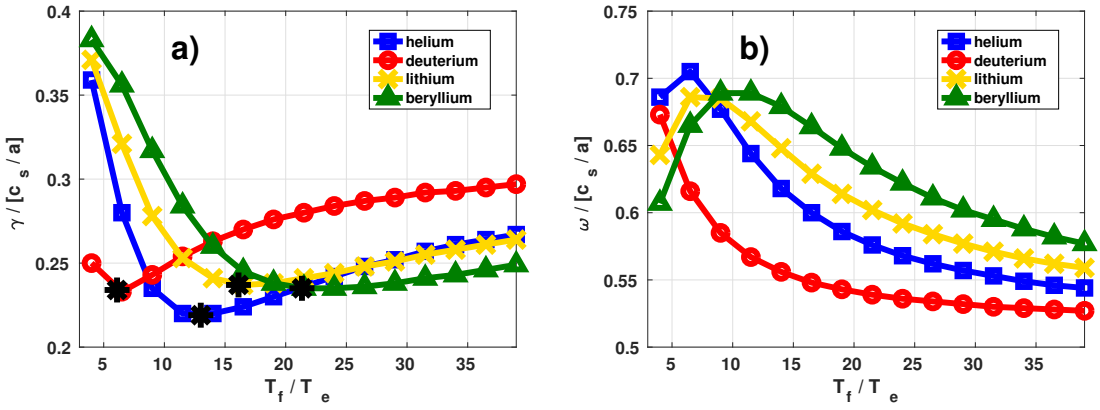

FIG. 13. a) Growth rates and b) frequencies as a function of the fast particle temperature T_f/T_e for different fast ion species at $k_y\rho_s = 0.5$. The fast particle charge concentration is fixed to $q_f n_f = 0.14 n_e$.

on the plasma geometry.

VII. NONLINEAR REGIME

The extension of the previous results to nonlinear regimes is an essential step toward assessing possible resonance mechanism related plasma confinement improvements. For this purpose, electrostatic turbulence simulations are performed with the gyrokinetic code GENE in the three species setup with deuterium, electron and helium. The physical parameters are the same as in Tab. I. The radial box size is $175\rho_s$ and the minimal $k_y\rho_s$ is set to 0.05. We used 192 grid points in radial direction and employed 48 modes in the binormal direction. Along the field line 24 points were used. In velocity space, 20 Gauss-Laguerre distributed magnetic moment knots and 32 equidistant symmetric parallel velocity grid points have been used. Fig. 14 shows the time traces of the thermal and energetic ion heat fluxes

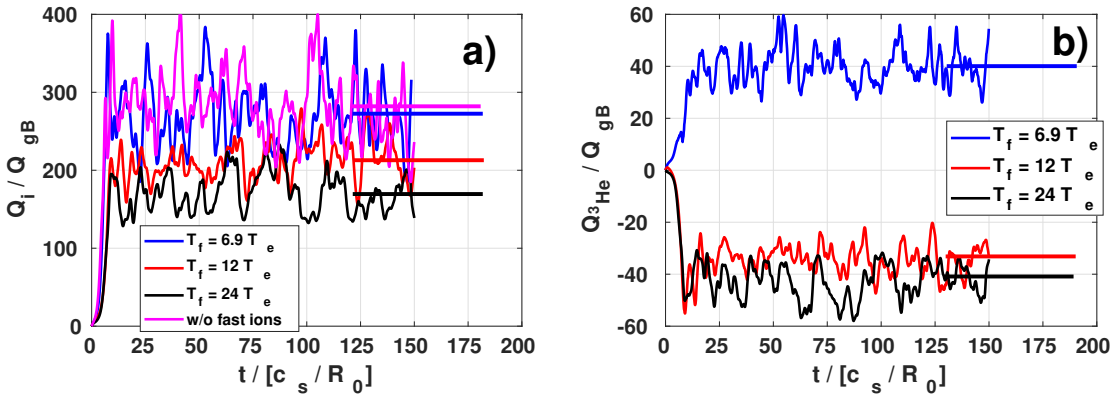

FIG. 14. Time trace of the nonlinear (a) main ion, (b) fast ion heat flux in GyroBohm units for different energetic particle temperature T_f/T_e and for the case with only thermal species.

expressed in gyroBohm $Q_{gB} = v_{th,i}\rho_i^2 n_e T_i/R_0^2$ normalized units for different fast particle temperatures. A strong reduction of the thermal deuterium flux is observed in correspondence to an increase in the fast particle temperature. This stabilization is maximized for $T_f = 24T_e$, consistently with the theoretical predictions of the resonant reduced model for the linear mode which is more unstable nonlinearly, namely $k_y\rho_s \sim 0.2$[13]. The energetic particle heat flux, on the other hand, is also found to reach a minimum for the same temperature, i.e. $T_f = 24T_e$. However, contrarily to the thermal species, Fig. 14 reveals negative fast ion heat transport where the wave-fast ion resonant interaction is predicted to be more effective. The generation of negative fluxes is particularly convenient for fusion reactors. They are related to radially inward energy injection and hence to an improvement of overall core-energy confinement.

Another striking observation is the nonlinear behavior of the cross phase relation (α) between the electrostatic potential and the main ion density perturbation. Dur-

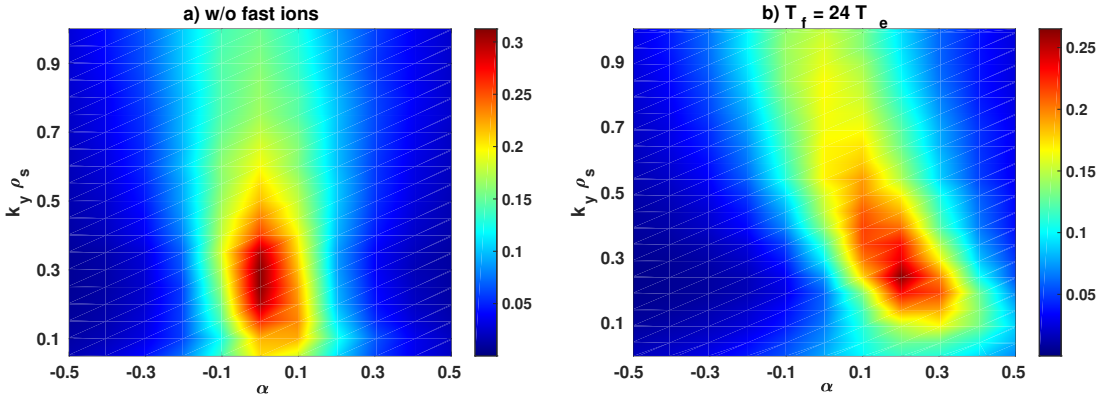

FIG. 15. Nonlinear cross phase (in rad) between the perturbed electrostatic potential and the main ion density perturbation at different $k_y\rho_s$, a) removing and b) including energetic particles at $T_f = 24T_e$. It is taken at $z = 0$ and in the steady-state time domain $t/[c_s/R_0] = [25 - 150]$.

ing the investigation of section II the linear cross phase was shown to be a function of the fast particle temperature and to be strongly affected by resonance effects between the main ITG mode and the energetic particles. Similar results are also observed in turbulent regimes in Fig. 15, where the cross phase function $\chi(\alpha, k_y\rho_s)$ obtained for $T_f = 24T_e$ is compared to the one without energetic particles. It is measured at $z = 0$ and is obtained by performing a time average in the steady-state domain $t/[c_s/R_0] = [25 - 150]$. Fig. 15 reveals that χ, which peaks as the nonlinear drive at $k_y\rho_s \sim 0.2$, is zero ($\alpha = 0$) if energetic particles are neglected. However, consistently with the linear results shown in Fig. 2, it increases significantly for the case $T_f = 24T_e$. In particular, each scale undergoes a different dephasing, consistently with the linear results on Fig. 4.

VIII. QUASI-LINEAR ENERGETIC ION HEAT FLUX DECOMPOSITION

The resonant interaction between energetic particles and ITG micro-instability is not significantly affected by cross-scale coupling. Its main features can be qualitative and quantitative captured even in the simplified single mode framework presented previously. This observation allows for deriving a quasi-linear description - following the analytic derivation of Ref. 30 and 31 - able to explain the temperature dependences of the energetic particle steady-state heat flux. In the gyrokinetic formalism, it is defined in the guiding center coordinate system $(\vec{x}, \vec{v})$ as

$$Q_{1,f} = \frac{m}{2} \int v_E^x v^2 F_{1,f}(\vec{x}, \vec{v}) d^3v, \tag{15}$$

where v_E^x represents the radial component of the $E \times B$ velocity, namely $v_E^x = \frac{c}{B_0^2} \left(\vec{B}_0 \times \vec{\nabla} \bar{\phi}_1 \right)_x$. The gyrokinetic representation of Eq. (15) in the $\shortparallel$-symplectic $(\alpha = 0, \beta = 1)$ model of Ref. 32 is obtained by employing the so-called pullback operator and removing any dependence on the gyro-angle. After an average in the perpendicular plane and a Fourier decomposition for the perturbed quantities, Eq. (15) can be rewritten in the GENE field-aligned coordinate system as follows

$$Q_{1,f} = -\Re \left\{ \sum_k \pi B_0 \frac{c}{\mathcal{C}} i k_y \int \left(v_{\shortparallel}^2 + \frac{2 B_0 \mu}{m_f} \right) J_0 \phi_1^k F_1^{k,*} dv_{\shortparallel} d\mu \right\}. \tag{16}$$

Here, the field-aligned representation of the radial component of the $E \times B$ velocity $v_E^x = -\frac{c}{\mathcal{C}} \partial_y \bar{\phi}_1$ has been employed. The radial fast particle heat flux can be further computed by means of the reduced Vlasov equation derived in Eq. (5), which in

normalized units reads

$$Q_{1,f}/Q_{gB} = \frac{\pi B_0 n_f T_f}{\mathcal{C}^2} \sum_{k_y} k_y^2 \left|\phi_1^k\right|^2 \gamma_\nu^k \int J_0^2 \left(v_{\shortparallel}^2 + \mu B_0\right) \frac{\left[\frac{R}{L_{n,f}} + \frac{R}{L_{T,f}}\left(v_{\shortparallel}^2 + \mu B_0 - \frac{3}{2}\right)\right] F_M}{\left(\omega_r + \frac{T_f}{q_f}\left(\frac{\mu B_0 + 2v_{\shortparallel}^2}{B_0}\right) k_y \mathcal{K}_y\right)^2 + \gamma_\nu^2} dv_{\shortparallel} d\mu. \tag{17}$$

Here, Eq. (17) is expressed in gyroBohm units. Following a similar approach as in Refs. 30 and 31 for the particle flux, Eq. (17) can be written in a quasi-linear framework as the sum of a off-diagonal diffusion D_n - proportional to the fast particle density gradient - and a diagonal-diffusion D_T - due to the presence of temperature gradients, i.e.

$$Q_{1,f}/(n_f T_f Q_{gB}) = D_n \frac{R}{L_{n,f}} + D_n \frac{R}{L_{T,f}}. \tag{18}$$

The quasi-linear decomposition of Eq. (18) can be easily identified in the reduced expression for the energetic particle heat flux derived in Eq. (17). The diffusion operators can hence be written as

$$D_n = \frac{\pi B_0 n_f T_f}{\mathcal{C}^2} \sum_{k_y} k_y^2 \left|\phi_1^k\right|^2 \gamma_\nu^k \int \frac{J_0^2 \left(v_{\shortparallel}^2 + \mu B_0\right) \frac{R}{L_{n,f}} F_{0,M}}{\left(\omega_r + \frac{T_f}{q_f}\left(\frac{\mu B_0 + 2v_{\shortparallel}^2}{B_0}\right) k_y \mathcal{K}_y\right)^2 + \gamma_\nu^2} dv_{\shortparallel} d\mu. \tag{19}$$

$$D_T = \frac{\pi B_0 n_f T_f}{\mathcal{C}^2} \sum_{k_y} k_y^2 \left|\phi_1^k\right|^2 \gamma_\nu^k \int J_0^2 \left(v_{\shortparallel}^2 + \mu B_0\right) \frac{\frac{R}{L_{T,f}}\left(v_{\shortparallel}^2 + \mu B_0 - \frac{3}{2}\right) F_{0,M}}{\left(\omega_r + \frac{T_f}{q_f}\left(\frac{\mu B_0 + 2v_{\shortparallel}^2}{B_0}\right) k_y \mathcal{K}_y\right)^2 + \gamma_\nu^2} dv_{\shortparallel} d\mu. \tag{20}$$

The above decomposition of the radial component of the fast particle heat flux reveals that the sign of the diffusion term depends on the sign of the density gradient. For the parameters employed throughout this work it is always positively defined, i.e. directed outward. Moreover, the sign of the diagonal-diffusion term depends

on the energetic particle temperature gradient and on the velocity space quantity $v_{\shortparallel}^2 + \mu B_0 - 3/2$. Its structure is of the same form as Eq. (14). Therefore, the resonance mechanism can affect the quasi-linear expression for $Q_{1,f}$ similarly as discussed previously for the linear contribution of the energetic ions to the total growth rate γ_f. Assuming positive values for the temperature gradient, a positive fast particle heat flux is expected when the linear contribution of the most unstable mode in the turbulence simulations (for these parameters $k_y \rho_i \sim 0.2$) is destabilizing. Negative fluxes, on the other hand, are expected in cases where the resonance moves to smaller energies in velocity space, therefore maximizing the negative contribution of the energetic particle drive. These theoretical predictions are confirmed by GENE nonlinear simulations for the three-species setup with fast helium. Fig. 16 shows indeed that the fast particle heat flux changes sign when the resonance position moves in phase space through more favorable regions, as discussed in sections II, III, IV for the linear growth rate analysis. In Fig. 16 the velocity space averaged growth rate contribution, normalized to the thermal deuterium one, is included in the lower right of each plots.

IX. CONCLUSIONS

Comprehensive numerical analyses have been performed and presented in the paper at hand to fully exploit the significant electrostatic stabilizing effects of energetic particles on plasma micro-turbulence. In particular, the description of the resonance mechanism proposed in Ref. 13 is here significantly extended. The mechanism by which energetic particles can strongly impact ion-dominated-turbulence scenarios when the fast ion magnetic drift frequency approaches the linear ITG frequency is further elucidated. The magnitude of this interaction, however, depends strongly on the particular scale considered. Linear gyrokinetic simulations were performed with

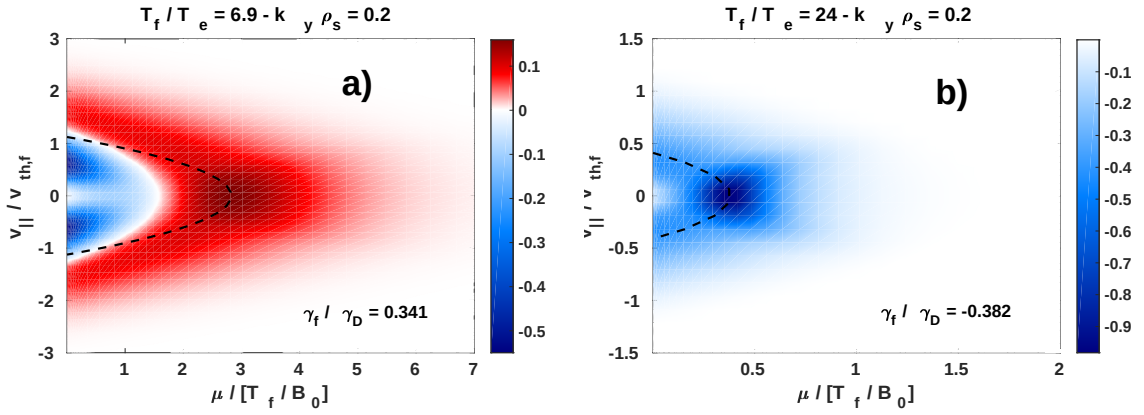

FIG. 16. Converged fast particle γ_f velocity space structure obtained from GENE at $z = 0$ for the $k_y\rho_s$ more relevant in turbulence simulations, i.e. $k_y\rho_s = 0.2$. The energetic particle temperature is taken as a) $T_f = 6.9T_e$ and b) $T_f = 24T_e$. The black contour lines indicate the resonance positions according to the reduced Vlasov model. Moreover, the velocity space averaged growth rate contribution, normalized to the thermal deuterium one, is included in the lower right of each plots.

the gyrokinetic code GENE to assess possible improvements. By employing realistic JET-like parameters, the effects of the magnetic shear and fast ion properties - mass and charge - have been studied. All the numerical results have been compared with the reduced theoretical expression of Ref. 13, which is here derived in details and allows to locate the phase-space $(v_{||}, \mu)$ positions where the interaction between fast ion and ITG micro-instability becomes more effective. The consequences of such mechanisms on the overall system free energy has also been modelled with a simplified expression for the energetic particle field and kinetic energy terms. The capabilities of such models to capture the modifications of the resonant interaction due to changes in the fast particle charge, mass and magnetic shear are shown. More precisely, negative values of the magnetic shear are found to further locate

the phase-space resonance position to smaller values of the field-align coordinate z, i.e. the ITG instability peaks, with a consequent enhancement of the resonance effects. Moreover, the mass and charge are shown to impact the wave-fast ion interaction in opposite ways. Contrary to the mass, an increase in the charge results in an enhancement of micro-turbulence suppression. Finally, the study of the resonant mechanism described in this paper is further extended to nonlinear regimes, i.e. including cross-scale coupling terms. The nonlinear features of the fast ion heat fluxes are also investigated and reproduced with a quasi-linear model, based on the simplified theory of Ref. 13, 30, and 31. It is shown that the resonance mechanism can affect the energetic particle heat flux, similarly as linear ITG growth rates. In particular, inward fluxes are observed in correspondence of the strongest fast ion stabilization. These results are perfectly captured with the quasi-linear model based on the reduced theoretical expression for the fast particle Vlasov equation. It may be used to give rough estimates on the relevance of electrostatic resonance effects of energetic particles on ITG-dominated turbulence.

ACKNOWLEDGEMENT

The simulations presented in this work were performed at the HYDRA HPC system at the Max Planck Computing and Data Facility (MPCDF), Germany. Furthermore, we acknowledge the CINECA award, for the availability of high performance computing resources and support. This work has been carried out within the framework of the EUROfusion Consortium and has received funding from the Euratom research and training programme 2014 - 2018 under grant agreement No 633053. The views and opinions expressed herein do not necessarily reflect those of the European Commission. The authors would like to thank N. Bonanomi, J. Citrin, E. Fable, Ph. Lauber, P. Mantica, F. Jenko for all the stimulating discussions, useful

suggestions and comments.

REFERENCES

[1]W. Horton, Rev. Mod. Phys **71** (1999), 10.1103/RevModPhys.71.735.

[2]F. Romanelli, Physics of Fluids B **1**, 1018 (1989).

[3]P. Mantica, D. Strintzi, T. Tala, C. Giroud, T. Johnson, H. Leggate, E. Lerche, T. Loarer, A. G. Peeters, A. Salmi, S. Sharapov, D. Van Eester, P. C. de Vries, L. Zabeo, and K.-D. Zastrow, Phys. Rev. Lett. **102**, 175002 (2009).

[4]P. Mantica, C. Angioni, C. Challis, G. Colyer, L. Frassinetti, N. Hawkes, T. Johnson, M. Tsalas, P. C. de Vries, J. Weiland, B. Baiocchi, M. N. A. Beurskens, A. C. A. Figueiredo, C. Giroud, J. Hobirk, E. Joffrin, E. Lerche, V. Naulin, A. G. Peeters, A. Salmi, C. Sozzi, D. Strintzi, G. Staebler, T. Tala, D. Van Eester, and T. Versloot, Phys. Rev. Lett. **107**, 135004 (2011).

[5]N. Bonanomi, P. Mantica, A. Di Siena, E. Delabie, T. Johnson, E. Lerche, S. Menumir, M. Tsalas, D. Van Eester, and JET Contributors, Nucl. Fusion **58**, 056025 (2018), 10.1088/1741-4326/aab733.

[6]G. Tardini, J. Hobirk, V. G. Igochine, C. F. Maggi, P. Martin, D. McCune, A. G. Peeters, A. C. C. Sips, A. Stäbler, J. Stober, and ASDEX Upgrade Team, Nucl. Fusion **47**, 280 (2007).

[7]M. Romanelli, A. Zocco, F. Crisanti, and JET Contributors, Plasma Phys. Controlled Fusion **52**, 045007 (2010).

[8]C. Holland, C. C. Petty, L. Schmitz, K. H. Burrell, G. R. McKee, T. L. Rhodes, and J. Candy, Nucl. Fusion **52**, 114007 (2012).

[9]J. Citrin, J. Garcia, T. Görler, F. Jenko, P. Mantica, D. Told, C. Bourdelle, D. R. Hatch, G. M. D. Hogeweij, T. Johnson, M. J. Pueschel, and M. Schneider, Plasma Phys. Controlled Fusion **57**, 014032 (2015).

[10]J. Citrin, F. Jenko, P. Mantica, D. Told, C. Bourdelle, J. Garcia, J. W. Haverkort, G. M. D. Hogeweij, T. Johnson, and M. J. Pueschel, Phys. Rev. Lett. **111**, 155001 (2013).

[11]C. Bourdelle, G. T. Hoang, X. Litaudon, C. M. Roach, and T. Tala, Nucl. Fusion **45**, 110 (2005).

[12]H. Doerk, A. Bock, A. Di Siena, E. Fable, T. Görler, F. Jenko, J. Stober, and The ASDEX Upgrade Team, Nucl. Fusion **58**, 016044 (2018).

[13]A. Di Siena, T. Görler, H. Doerk, E. Poli, and R. Bilato, Nucl. Fusion **58**, 054002 (2018).

[14]A. Di Siena, T. Görler, E. Poli, A. Bañón Navarro, A. Biancalani, and F. Jenko, Arxiv (2018), arXiv:1812.03755.

[15]G. J. Wilkie, A. Iantchenko, I. G. Abel, E. Highcock, I. Pusztai, and JET Contributors, Nucl. Fusion **58**, 082024 (2018).

[16]F. Jenko, W. Dorland, M. Kotschenreuther, and B. N. Rogers, Phys. Plasmas **7**, 1904 (2000).

[17]R. Bravenec, J. Citrin, J. Candy, P. Mantica, T. Görler, and JET Contributors, Plasma Phys. Controlled Fusion **58** (2016), 10.1088/0741-3335/58/12/125018.

[18]A. Zocco, P. Xanthopoulos, H. Doerk, J. W. Connor, and P. Helander, J. Plasma Phys **84**, 715840101 (2018).

[19]A. Di Siena, T. Görler, H. Doerk, J. Citrin, T. Johnson, M. Schneider, E. Poli, and JET Contributors, J. Phys. Conf. Ser. **775**, 012003 (2016).

[20]A. Di Siena, T. Görler, H. Doerk, R. Bilato, J. Citrin, T. Johnson, M. Schneider, E. Poli, and JET Contributors, Phys. Plasmas **25**, 042304 (2018).

[21]A. Di Siena, A. Biancalani, T. Görler, H. Doerk, I. Novikau, P. Lauber, A. Bottino, E. Poli, and The ASDEX Upgrade Team, Nucl. Fusion **58**, 106014 (2018).

[22]R. Miller, M. Chu, J. Greene, Y. Lin-Liu, and R. Waltz, Phys. Plasmas **5**, 979 (1998).

[23]T. Görler, X. Lapillonne, S. Brunner, T. Dannert, F. Jenko, F. Merz, and D. Told, Journal of Computational Physics **230**, 7053 (2011).

[24]T. Dannert, S. Günter, T. Hauff, F. Jenko, X. Lapillonne, and P. Lauber, Phys. Plasmas **15**, 062508 (2008).

[25]C. Angioni and A. G. Peeters, Phys. Plasmas **15**, 052307 (2008).

[26]R. Hatzky, T. M. Tran, A. Könies, R. Kleiber, and S. J. Allfrey, Phys. Plasmas **9**, 898 (2002).

[27]A. Bañón Navarro, P. Morel, M. Albrecht-Marc, D. Carati, F. Merz, T. Görler, and F. Jenko, Phys. Plasmas **18**, 092303 (2011).

[28]A. Bañón Navarro, P. Morel, M. Albrecht-Marc, D. Carati, F. Merz, T. Görler, and F. Jenko, Phys. Rev. Lett. **106**, 055001 (2011).

[29]P. Manas, Y. Camenen, S. Benkadda, W. A. Hornsby, and A. G. Peeters, Phys. Plasmas **22**, 062302 (2015).

[30]T. Hein, C. Angioni, E. Fable, and J. Candy, Phys. Plasmas **17**, 102309 (2010).

[31]C. Angioni, Y. Camenen, F. J. Casson, E. Fable, R. M. McDermott, A. G. Peeters, and J. E. Rice, Nucl. Fusion **52**, 114003 (2012).

[32]A. J. Brizard and T. S. Hahm, Rev. Mod. Phys. **79**, 421 (2007).